Long-term Land-Atmosphere Energy and Water Exchange Observational Dataset over central Tibetan Plateau

Haipeng Yu[1], Guantian Wang[2], Zeyong Hu[1]*, Yaoming Ma[3], Maoshan Li[4], Weiqiang Ma[3], Lianglei Gu[1],

Fanglin Sun[1], Hongchun Gao[1], Shujin Wang[1], Fuquan Lu[1,5]

[1] Nagqu Plateau Climate and Environment Observation and Research Station of Tibet Autonomous Region, State Key Laboratory of Cryospheric Science and Frozen Soil Engineering, Northwest Institute of Eco-Environment and Resources, Chinese Academy of Sciences, Lanzhou 730000, China

[2]Tianjin Meteorological Observatory, Tianjin 300202, China

[3]Land-Atmosphere Interaction and Its Climatic Effects Group, State Key Laboratory of Tibetan Plateau Earth System, Environment and Resources, National Observation and Research Station for Qomolongma Special Atmospheric Processes and Environmental Changes, Institute of Tibetan Plateau Research, Chinese Academy of Sciences, Beijing 100101, China

[4]School of Atmospheric Sciences, Plateau Atmosphere and Environment Key Laboratory of Sichuan Province, Chengdu Plain Urban Meteorology and Environment Observation and Research Station of Sichuan Province, Chengdu University of Information Technology, Chengdu 610225, China[5]University of Chinese Academy of Sciences, Beijing 100049, China

Correspondence: Zeyong Hu (zyhu@lzb.ac.cn)

Abstract: In recent decades, the climate of Tibetan Plateau has undergone notable changes, which has a strong influence on global climate systems and human activities, making it a research hotspot. However, due to its extreme elevation, harsh environment, and complex underlying surface, long-term observations of the central Plateau's atmospheric vertical profiles have been challenging and scientific data sharing is crucial and in urgent need. This paper presents a 9-year observational dataset (2014-2022) with hourly temporal resolution from the Nagqu region of northern Tibet. The dataset is a combination of four field stations covering the central Tibetan Plateau, which recorded near-surface meteorological data, radiation budget, turbulent fluxes, and soil hydrothermal characteristics. All observational items in this dataset underwent data processing and quality control to ensure data quality. This dataset represents the most detailed raw observational data on the central Tibetan Plateau's spatial coverage and recent changes. It holds significant value in revealing energy and water exchanges between the land surface and the atmosphere on the Tibetan Plateau. Main datasets are freely available at the National Tibetan Plateau / Third Pole Environment Data Center (https://doi.org/10.11888/Meteoro.tpdc.270010 and https://cstr.cn/18406.11.Meteoro.tpdc.270010, Hu et al., 2019) and additionally at National Tibetan Plateau / Third Pole Environment Data Center (https://doi.org/10.11888/Atmos.tpdc.300325 and https://cstr.cn/18406.11.Atmos.tpdc.300325, Hu et al., 2023).

38

Key words: field observation, observational dataset, land-atmosphere interaction, Tibetan Plateau, energy and water exchanges

41

1.Introduction

The Tibetan Plateau (TP), with an average altitude exceeding 4000 meters, is the world's largest mountain range, often referred to as the "Third Pole" (Qiu, 2008). It is the source of many major rivers, including the Yangtze, Yellow, Mekong, and Brahmaputra, which provide freshwater to 1.4 billion people (Immerzeel et al., 2020). It is also known as the "Asian Water Tower" (Immerzeel et al., 2010). The plateau's substantial absorption of solar radiation renders it the warmest region in the mid-troposphere. This plays a key role in the evolution of the East Asian Summer Monsoon and Indian Summer Monsoon systems (Wu et al., 2007; Wu et al., 2012; Li et al., 2018; Zhang et al., 2019), which in turn affect circulation patterns in East Asia, and even the Northern Hemisphere (Fan et al., 2023; Curio and Scherer, 2016; Sun et al., 2022). The intricate surface characteristics of the TP make it particularly susceptible to external disturbances in the context of global warming (Li et al., 2022; Kang et al., 2010). Meteorological observations indicate that surface warming on the TP commenced at an earlier and more accelerated pace than in other regions at the same latitude (Liu and Chen, 2000). Climate change on the TP has resulted in most regions becoming warmer and moister, while the southern part has become warmer and drier (Yang et al., 2014). These changes in temperature and moisture have further led to significant shifts in many environmental systems on the plateau, including precipitation (Yang et al., 2011), glaciers (Yao et al., 2012), lakes (Lei et al., 2014), and vegetation (Shen et al., 2015). Therefore, in-depth research on TP not only helps us better understand the impact of global warming on its unique ecosystems and climatic features, but also is crucial for assessing its contribution to regional and even global water cycles and energy balance. In recent decades, a multitude of comprehensive observation stations have been established with the objective of strengthening climate change research on the TP. These include the Third Pole Environment Observation and Research Platform and the Integrated Three-Dimensional Observation Research Platform for Third Pole Environment (Ma et al., 2018; Ma et al., 2023). The establishment of these observation stations has resulted in a significant improvement in the availability of data on land-atmosphere interactions on the plateau. The comprehensive data network has enhanced the quality of land surface models and corrected satellite retrievals (Ma et al., 2023). However, due to factors such as transportation and maintenance costs, most observations are concentrated in the eastern part of the TP, with limited long-term observations of the plateau's interior, especially in the high-altitude regions of northern Tibet (Shen and Xiong,2016; Duan and Xiao, 2015).

The central Tibetan Plateau (CTP) belongs to a typical plateau climate with an average altitude exceeding 4500 metres. It is bordered by the Kunlun and Tanggula Mountains to the northwest and the Nyenchen Tanglha Mountains to the south, covering an area of 446,000 square kilometres, which represents one-fifth of the total area of Tibet. The CTP is known as the "Roof of the Roof of the World," representing the highest and most typical plateau form on the TP. Due to its high altitude, the substrate is dominated by cold-resistant vegetation, with an annual precipitation of 154.9 mm and approximately 50 rainy days, characterizing a typical subarctic semi-arid monsoon climate (Li et al., 2017). During clear weather, the downward shortwave radiation peaks at 1200 W/m², which is significantly higher than inland observations (He et al., 2010). The period from May to September is characterised by warm and moist conditions, with frequent rainfall, while October to April is cold and dry with prevalent strong winds. During the summer months, the CTP serves as a thermal core area, with surface heating being a key factor in making the plateau a heat source. The thermal effect of the CTP influences not only the plateau itself but also weather and climate systems in East Asia, and even the Northern Hemisphere (Zhao et al.,2019). Over the past 40 years, the warming trend on the CTP has been significantly higher than in lower-altitude areas, with surface temperature warming rates and

precipitation amounts also higher than in eastern regions of the TP (Chen et al., 2003; Liu et al., 2009; Yang et al., 2002). The number of consecutive dry days on the central TP has been steadily decreasing in conjunction with accelerated warming and moistening (Ciwangdunzhu et al., 2018), while its lakes are experiencing strong expansion or contraction (Zhang et al., 2019; Lei et al., 2013 Lei et al., 2014). Some lakes serve as heat sources year-round and have an annual evaporation rate of 312.9mm (Guo et al., 2014). Concurrently, glaciers on the CTP are rapidly melting, and permafrost areas are shrinking, severely impacting the surrounding environment (Jin et al., 2009; Sun et al., 2020). A substantial evidence base indicates that the CTP 's ecological environment is highly fragile, and the surface heat exchange in this region is significant for climate change. However, there remains substantial uncertainty regarding the impact mechanisms (Song et al., 2012; Yang et al., 2014). This can be attributed to the harsh environment, frequent extreme weather such as strong winds and hail showers, and faulty observation equipment. Furthermore, much of the region's intricate topography is unsuitable for human habitation, resulting in a sparsely populated area, inadequate transportation infrastructure, and delayed equipment maintenance. This has led to the availability of relatively limited long-term and stable observational data for the CTP.

To fill these gaps, a series of mesoscale observation networks have been established in the vicinity of the Nagqu Observation Network of Plateau Climate and Environment (NPCE) (Xu et al., 2013). The NPCE commenced observations in 1997 and serves as a link between the East Asian Monsoon and the Indian Monsoon, as well as a transition zone between the monsoon systems and westerly circulation. It is a region of significant thermal activity on the plateau, and the central zone for China's Third Atmospheric Science Experiment on the TP. This distinctive geographical position gives NPCE a pivotal role in TP research. Following decades of observations, data from the Nagqu observing network has become an important platform for research on land-atmosphere interactions in northern Tibet. It has provided significant support for studies on boundary layer observations (Gu et al., 2022; Ueno et al., 2012), land-atmosphere energy transfer (Yang et al., 2010; Gu et al., 2015; Li et al., 2015), substrate evaporation (Zou et al., 2018), soil hydrothermal balance (Bian et al., 2012; Fu et al., 2022), and numerical simulations (Deng et al., 2021; Li et al., 2009; Sun et al., 2020). In recent years, there has been a gradual increase in the availability of field datasets to the public with free access. In order to optimise the potential value of scientific datasets, we describe and provide a high-time-resolution dataset. This dataset comprises nine years of near-surface meteorological, radiation, turbulent flux, and soil hydrothermal observations from NPCE. It provides a more accurate and comprehensive depiction of land-atmosphere interactions and boundary layer structure on the TP, playing a key role in numerical simulations and climate assessments.

The paper is organized as follows: Section 2 provides an overview of NPCE's geographic location, observation equipment, variables, data processing, and data availability. Section 3 presents near-surface meteorological, radiation, turbulent flux, and soil hydrothermal observations, discussing data integrity. Section 4 comprises a discussion, and Section 5 is conclusion.

2. Observation network and data processing

2.1 Site descriptions

The NPCE is affiliated with the Northwest Institute of Eco-Environment and Resources, Chinese Academy of Sciences, was established on 4 May 2009, with observational activities commencing on 1 April 1997. The central station is situated in Niaoqu Village, Luoma Town, Seni District, Nagqu City, Tibet Autonomous Region (longitude 91.90° E, latitude 31.37° N, altitude 4509 metres), near the

Tanggula Mountains, where the Indian monsoon and the East Asian monsoon intersect. The observation field is relatively flat and open, with abundant water resources and situated in an area characterised by pastoral activities. The substrate vegetation is primarily alpine grassland, with a relatively clean atmosphere and a low aerosol content. The station's unique geographic location and subsurface characteristics are significant for the observation and study of high-altitude climate environments.

Over more than 20 years, NPCE has developed into a network of four atmospheric boundary layer physics and land surface process observation points in the Nagqu region and along the Qinghai-Tibet Highway. The locations in Figure 1 are BJ, Amdo, NewD66, and MS3478. These represent different substrate characteristics, namely plateau grassland, plateau meadow, plateau wetland, and plateau bareland. Since plant roots are primarily concentrated in the shallow soil layers of the plateau, root biomass in the 0–10 cm layer accounts for 70% of the total root biomass (Su et al., 2021). This leads to pronounced seasonal variations in the surface soil at each observation site. In addition to vegetation, variations in soil temperature and moisture are influenced by precipitation, soil properties, and underlying permafrost. The correlation between soil temperature and air temperature gradually decreases with increasing depth (Wang et al., 2023). Consequently, the different underlying surfaces within the Nagqu observation network represent distinct environmental features of the TP, their interannual variation trends and influencing factors exhibit notable differences (Sun et al., 2015). In 2014, NPCE became a member of the Chinese Academy of Sciences Cold Region Surface Process and Environmental Monitoring Research Network and the Chinese Academy of Sciences Land Surface Process Research Network.
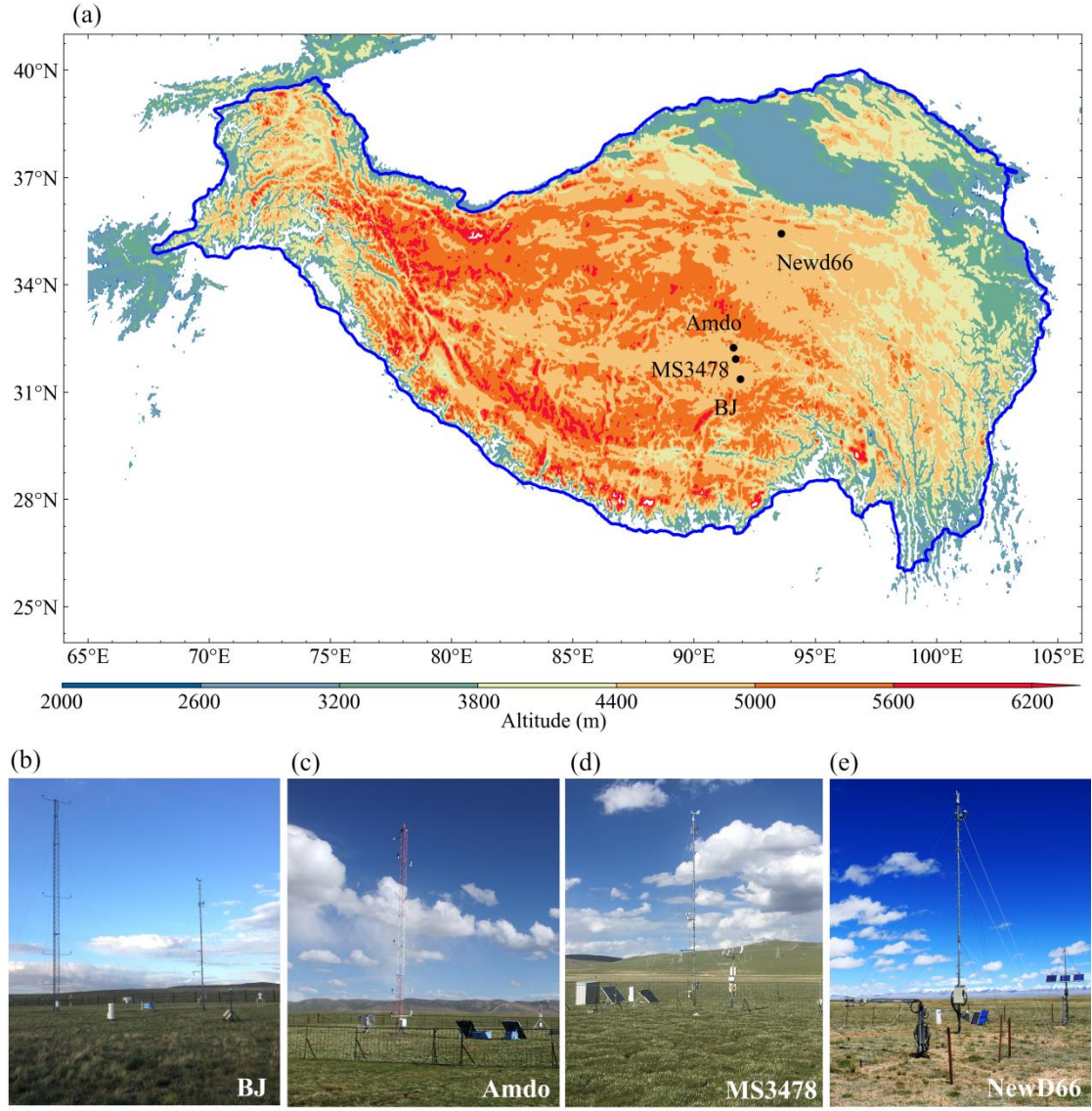
Figure 1. Geographic locations of the observation stations of NPCE (a) and on-site image of BJ (b), Amdo (c), MS3478 (d), and NewD66 (e).

2.2 Observation infrastructure and data processing

The NPCE utilises automatic observation mode, capable of sustaining continuous observation throughout the year. In order to ensure the continuity and accuracy of the observation data, the maintenance engineers are responsible for conducting on-site inspections and maintenance of the infrastructures at regular intervals at each observation station and collect the observation data. All data are transmitted to the data centre for processing to facilitate timely and effective detection of technical problems.

The NPCE near-surface meteorological observation system consists of Planetary Boundary Layer (PBL) towers and Automatic Weather Stations (AWS). These instruments measure vertical profiles of meteorological conditions, including air temperature, relative humidity, wind direction and wind speed within the boundary layer. Observation heights range from 0.75-12 m at BJ and Amdo, and

169 approximately 1 m and 10 m at NewD66 and MS3478. The observation probes deployed at each station
170 were of the same type to ensure consistency, but the specific observation heights varied slightly across
171 different stations. The vertical soil hydrothermal characteristics were measured at each station with
172 multilayer soil temperature and moisture probes located between 5-160 cm from the surface, with a
173 proportional distribution of observation depths. High-frequency Eddy Covariance (EC) systems were
174 installed at the four stations after 2012, allowing for the capture of sensible, latent and carbon dioxide
175 fluxes, with a sampling frequency of 0.1 s and an output interval of 30 minutes. Surface observations
176 encompass surface air temperature, humidity, radiative quadrature, atmospheric pressure, precipitation,
177 and snow depth. All observations are recorded at a sampling frequency of 10 seconds and an output
178 interval of 30 minutes. More details of the observation instruments are listed in Table 1. Station BJ is
179 also equipped with a ground-based microwave radiometer, a blowing snow observation instrument, and
180 a wind profile radar. The ground-based microwave radiometer (MWP967KV) can observe temperature
181 and humidity profiles up to 10 km above the surface under all weather conditions, with a 2-minute
182 output interval. The FlowCapt FC4 blowing snow sensor inverts digital signals by collecting the
183 acoustic pressure of the blowing snow particles as they impact. The CFL-03 pulsed Doppler wind
184 profile radar (WPR) can capture the wind speed and wind direction profile. It has a detection range of
185 300 to 3,000 metres and an output interval of 5 minutes. These observational instruments collectively
186 constitute a well-established monitoring system capable of comprehensively tracking weather events
187 across the central TP and their associated impacts.

188 For near-surface micrometeorological observations in complex environments, quality control of
189 data processing is crucial. In order to ensure the consistency of data at each site in the harsh natural
190 environment of the TP, engineers firstly check the data in terms of range, which is a constant value set
191 according to the climatic conditions of the TP and ignore the seasonal variations. Factors such as the
192 replacement of original parts and extreme weather can lead to temporary sensor malfunction. This can
193 result in no change or unrealistic jumps in the data for several hours. These factors can make it difficult
194 to properly deal with the issue during the range check. Consequently, engineers will utilise manual
195 quality control at the conclusion of the process, based on empirical observations, to rectify or eliminate
196 anomalous intervals and thereby ensure that outliers do not adversely affect the mean observations. The
197 removed missing measurements and outliers are denoted by NAN or -9999. Moreover, three categories
198 of quality classification are employed for turbulent fluxes. 0 denotes the highest quality of flux, 1
199 denotes flux suitable for general analysis, and 2 denotes flux with possible anomalies.

200   Table 1. Detailed information about observation stations and instruments of NPCE.

Site	Variables	Sensor models	Manufacturers	Observation period	Installation height/depth (m)	Units
BJ Lat: 31.37°N Lon: 91.90°E Location:Nagqu Altitude: 4509 m Established in 2001 Plateau Grassland	Air temperature	HMP45D	Vaisala	2001-2018	1.0/2.0/4.0/8.0/16.0/24.0	°C
		HMP155	Vaisala	2012-2022	0.75/1.5/3.0/6.0/12.0/22.0	
	Wind speed and direction	A-5400	Komatsu	2001-2018	10.36	m/s
		WindSonic	Gill	2012- 2022	0.75/1.5/3.0/6.0/12.0/22.0	
	Relative humidity	HMP45D	Vaisala	2001-2018	1.0/2.0/4.0/8.0/16.0/24.0	%
		HMP155	Vaisala	2012-2022	0.75/1.5/3.0/6.0/12.0/22.0	
	Precipitation	NOAH-II	ETI	2001-2018	1.00	mm
		T-200B	Geonor	2012-2022	1.00	
	Soil temperature	TS-301	Okazaki	2001-2018	-0.04/-0.10/-0.20/-0.40	°C
		TR-219	Truwel	2012-2022	-0.05/-0.10/-0.20/-0.40/-0.80/-1.60	
	Soil volumetric water content	Trime EZ	IMKO	2001-2018	-0.04/-0.20	m^{-3}/m^{-3}
		CS616	Campbell	2012-2022	-0.05/-0.10/-0.20/-0.40/-0.80/-1.60	
	Pressure	PTB220C	Vaisala	2001-2022	0.50	hPa
	Downward shortwave radiation	CM21	Kipp&Zonen	2001-2022	1.50	W/m^2
	Upward shortwave radiation	CM21	Kipp&Zonen	2001-2022	1.50	W/m^2
	Downward longwave radiation	PIR	Eppley	2001-2022	1.50	W/m^2
	Soil heat flux	MF-81	EKO	2001-2022	-0.05/-0.10	W/m^2
	Upward longwave radiation	PIR	Eppley	2001-2022	1.50	W/m^2
	Surface sensible heat flux	CSAT3 LI7500A	CAMPBELL CAMPBELL	2008-2022	3.00	W/m^2
	Surface latent heat flux	HMP45AC	VAISALA			

	CO$_2$/ H$_2$O Gas Analyzer	LI7500A	CAMPBELL	2022-2025	3.00	mg/m^3
Amdo Lat: 32.24°N Lon: 91.62°E Location:Amdo Altitude: 4695 m Established in 1997 Plateau Meadow	Air temperature	HMP155	Vaisala	2012-2022	1.5/3.0/6.0/12.0	°C
	Wind speed and direction	WindSonic	Gill	2012-2022	1.5/3.0/6.0/12.0	m/s
	Relative humidity	HMP155	Vaisala	2012-2022	1.5/3.0/6.0/12.0	%
	Precipitation	T-200B	Geonor	2012-2022	1.00	mm
	Soil temperature	TR-219	Truwel	2012-2022	-0.05/-0.10/-0.20/-0.40/-0.80/-1.60	°C
	Soil volumetric water content	CS616	Campbell	2012-2022	-0.05/-0.10/-0.20/-0.40/-0.80/-1.60	m^3/m^3
	Pressure	PTB220C	Vaisala	2001-2022	0.50	hPa
	Downward shortwave radiation	MS-801	EKO	2012-2022	1.50	W/m^2
	Upward shortwave radiation	MS-801	EKO	2012-2022	1.50	W/$^{-2}$
	Downward longwave radiation	PIR	EPPLEY	2012-2022	1.50	W/m^2
	Upward longwave radiation	PIR	EPPLEY	2012-2022	1.50	W/m^2
	Soil heat flux	MF-81	EKO	2012-2022	-0.05/-0.10	W/m^2
	Surface sensible heat flux Surface latent heat flux	CSAT3 LI7500A HMP45AC	CAMPBELL CAMPBELL VAISALA	2012-2022	3.00	W/m^2
	CO$_2$/ H$_2$O Gas Analyzer	LI7500A	CAMPBELL	2012-2022	3.00	mg/m^3
MS3478 Lat: 31.93°N Lon: 91.71°E Location:Liangdaohe Altitude: 4620 m Established in 2001 Plateau Wetland	Air temperature	HMP45D	Vaisala	2001-2022	0.85/9.35	°C
	Wind speed and direction	A-5400	Komatsu	2001-2022	10.35	m/s
	Relative humidity	HMP45D	Vaisala	2001-2022	0.85/9.35	%
	Precipitation	NOAH-II	ETI	2001-2022	1.00	mm
	Soil temperature	TS-301	Okazaki	2001-2022	-0.04/-0.10/-0.20/-0.40	°C
	Soil volumetric water content	Trime EZ	IMKO	2001-2022	-0.04/-0.20	m^3/m^3
	Pressure	PTB220C	Vaisala	2001-2022	0.5	hPa
	Downward shortwave radiation	CM21	Kipp&Zonen	2001-2022	1.50	W/m^2
	Upward shortwave radiation	CM21	Kipp&Zonen	2001-2022	1.50	W/m^2
	Downward longwave radiation	PIR	Eppley	2001-2022	1.50	W/m^2
	Upward longwave radiation	PIR	Eppley	2001-2022	1.50	W/m^2
	Surface sensible heat flux Surface latent heat flux	CSAT3 LI7500A HMP45AC	CAMPBELL CAMPBELL VAISALA	2012-2022	3.00	W/m^2
	CO$_2$/ H$_2$O Gas Analyzer	LI7500A	CAMPBELL	2012-2022	3.00	mg/m^3
NewD66 Lat: 35.43°N Lon: 93.59°E Location:Kekexili Altitude: 4465 m Established in 1997 Relocate in 2006 Plateau Bareland	Air temperature	HMP45D	Vaisala	1997-2022	0.60/9.30	°C
	Wind speed and direction	W955-FE	Komatsu	1997-2022	10.40	m/s
	Relative humidity	HMP45D	Vaisala	1997-2022	0.60/9.30	%
	Precipitation	NOAH-II	ETI	1997-2022	1.00	mm
	Soil temperature	TS-301	Okazaki	1997-2022	0.00/-0.01/-0.02/-0.03/-0.04/-0.06/-0.08/-0.10/-0.15/-0.20/-0.40/-0.60/-0.80/-1.00/-1.30/-1.60/-2.00/-2.12	°C
	Soil volumetric water content*	Trime EZ	IMKO	1997-2022	-0.011/-0.04/-0.075/-0.20/-0.40/-0.60/-0.80/-1.00/-1.60/-2.06	m^{-3}/m^{-3}
	Pressure	PTB210	Vaisala	1997-2022	0.5	hPa
	Downward shortwave radiation	CM21	Kipp&Zonne	1997-2022	1.50	W/m^2
	Upward shortwave radiation	CM21	Kipp&Zonne	1997-2022	1.50	W/m^2
	Downward longwave radiation	PIR	Eppley	1997-2022	1.50	W/m^2
	Upward longwave radiation	PIR	Eppley	1997-2022	1.50	W/m^2
	Soil heat flux	MF-81	EKO	1997-2022	-0.05/-0.10	W/m^2
	Surface sensible heat flux* Surface latent heat flux*	CSAT3 LI7500A HMP45AC	CAMPBELL CAMPBELL VAISALA	2012-2022	3.00	W/m^2
	CO$_2$/ H$_2$O Gas Analyzer	LI7500A	CAMPBELL	2012-2022	3.00	mg/m^3

201 Note: All data presented herein exhibit availability greater than 50%, with the mark '*' specifically
202 indicating availability below 80%.

203

204 **3. Data description**

205 **3.1 Near-surface meteorological data (Air temperature, relative humidity, wind speed)**

206
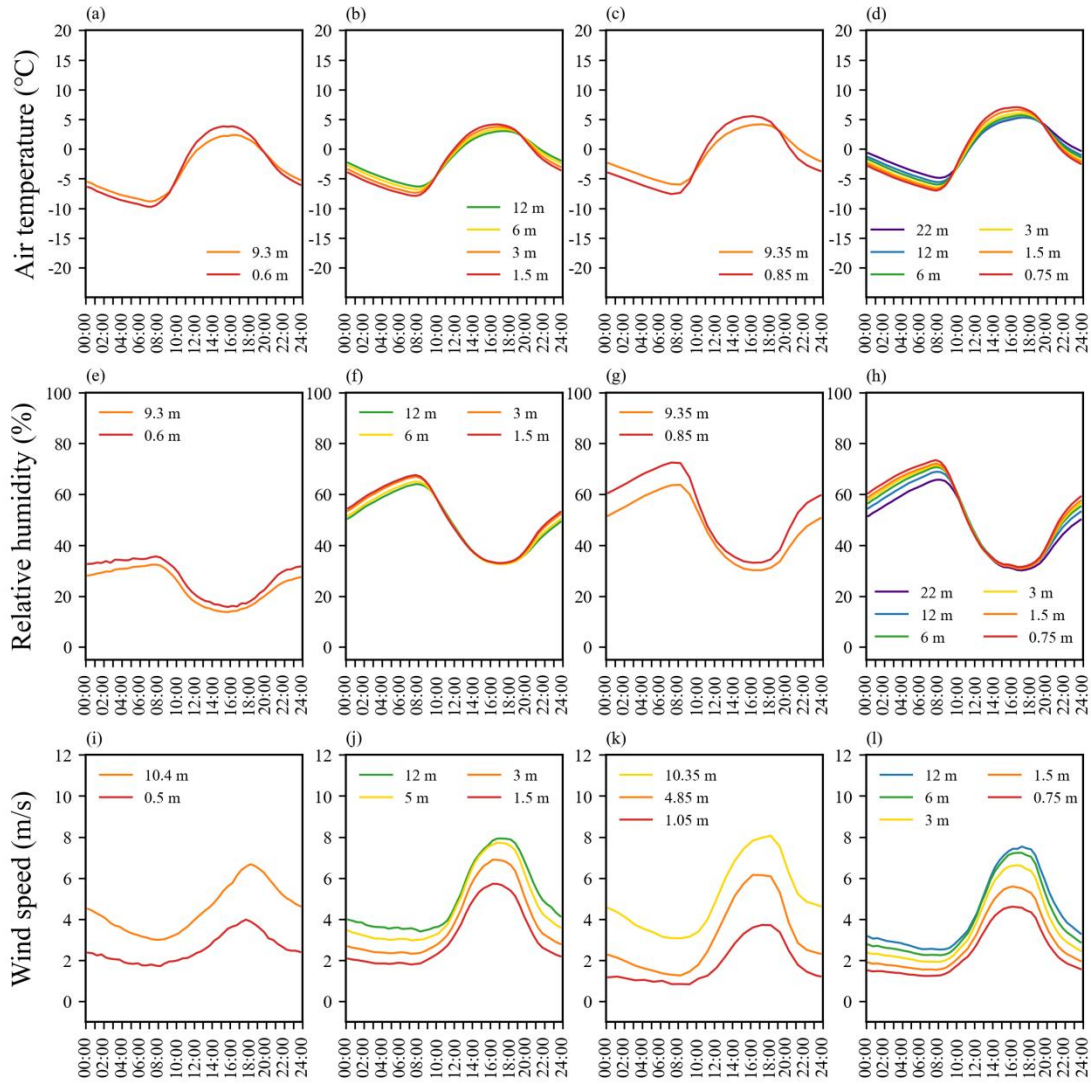
207 Figure 2. Diurnal variations of temperature at different heights of the PBL tower at NewD66 (a), Amdo

208 (b), MS3478 (c) and BJ (d), with corresponding relative humidity (efgh) and wind speed (ijkl) at each

209 station.

210

211   The main variables measured in near-surface micrometeorology are surface temperature, relative

212 humidity and wind speed. Surface air pressure is a single-level observation, which decreases with

213 altitude, while the other variables are gradient observations. Fig. 2 compares the diurnal cycles of

214 temperature, relative humidity and wind speed at different sites to illustrate the micrometeorological

215 characteristics influenced by the different underlying surfaces. Most sites exhibit a maximum

216 temperature at 18:00 and a minimum at 09:00, indicating a clear diurnal pattern. As a result of

217 latitudinal effects, the average temperature at the stations increases from north to south. The

218 northernmost station NewD66 records a minimum temperature of -9.73 ℃ and a maximum of 3.84 ℃,

219 while the southernmost station BJ records a minimum temperature of -7.02 ℃ and a maximum of

220 7.05 ℃. Irrespective of the water vapour content, relative humidity tends to decrease during the day

221 and increase at night. The most pronounced diurnal variations are observed at lower altitudes. This is

222 because daytime solar radiation heats the surface and atmosphere, making it harder for lower air layers

223 to saturate, which naturally reduces relative humidity. The wind speed generally increases with altitude

224 and shows a diurnal variation, being lower at night and higher during the day. MS3478 is situated in a
225 plateau wetland, where the abundance of vegetation increases friction with the underlying surface,
226 resulting in significantly reduced surface wind speeds at this station in comparison to other
227 locations.
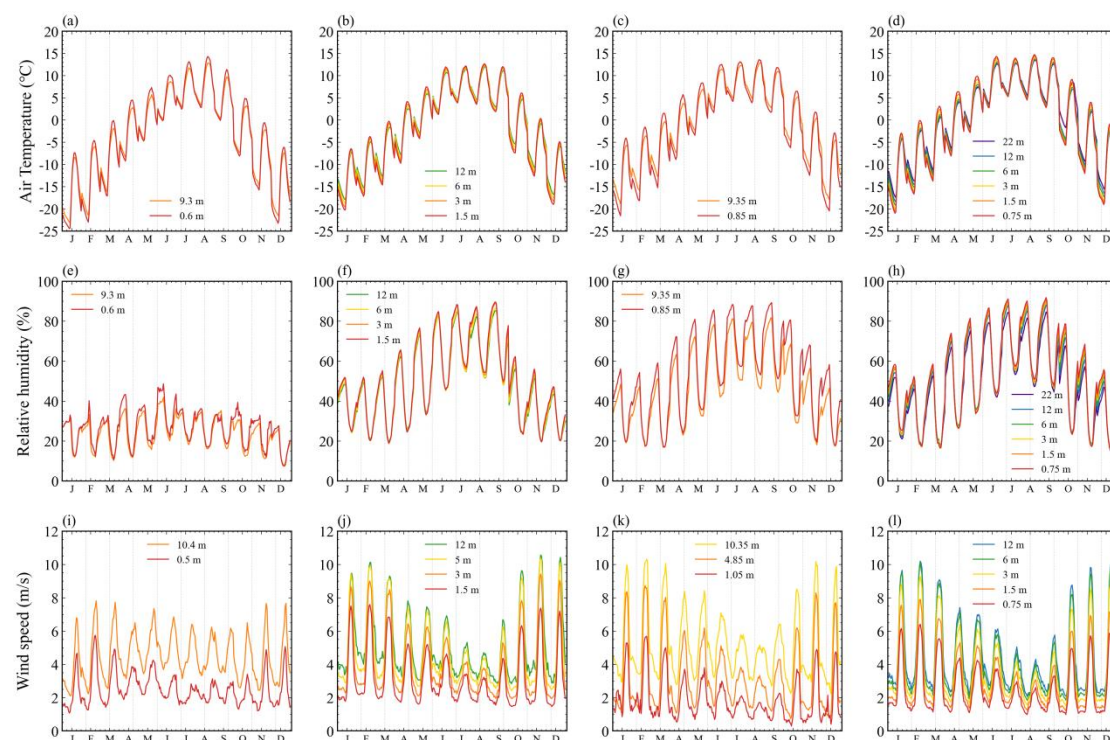
228
229 Figure 3. Monthly diurnal variations of temperature at different heights of the PBL tower at NewD66
230 (a), Amdo (b), MS3478 (c) and BJ (d), with corresponding relative humidity (efgh) and wind speed
231 (ijkl) at each station.

232
233 Most stations exhibited notable seasonal fluctuations in temperature, relative humidity and wind
234 speed (Fig. 3). Due to its cold bareland substrate, the NewD66 station experiences more pronounced
235 diurnal temperature variations, with nighttime temperatures lower than those observed at other stations,
236 occasionally reaching below -20 ℃ in January. In summer, with less pronounced diurnal variations
237 than in winter, temperatures peak at all sites, reaching approximately 13 ℃ during the day and
238 approximately 6 ℃ at night. Diurnal variations in relative humidity also show seasonal patterns, with
239 NewD66 remaining consistently lower, never exceeding 50%, and showing small variations in spring
240 and even smaller variations in summer. In contrast, the most pronounced diurnal variations in relative
241 humidity are observed during the spring at the other stations. As water vapour increases over the
242 plateau, nighttime relative humidity remains above 50% at all sites in summer, with diurnal humidity
243 variations gradually decreasing. Wind speeds show greater diurnal variation in winter and increase with
244 altitude. Peak wind speeds of more than 10 m/s are observed at the Amdo and BJ stations. In summer,
245 the 12 m wind speed at the Amdo and BJ sites peaks at 4.31 m/s in August. Surface wind speeds at
246 MS3478 are consistently low, but upper-level wind speeds are similar to those observed at the other
247 sites. Consequently, MS3478 exhibits the most pronounced gradient in wind speed.
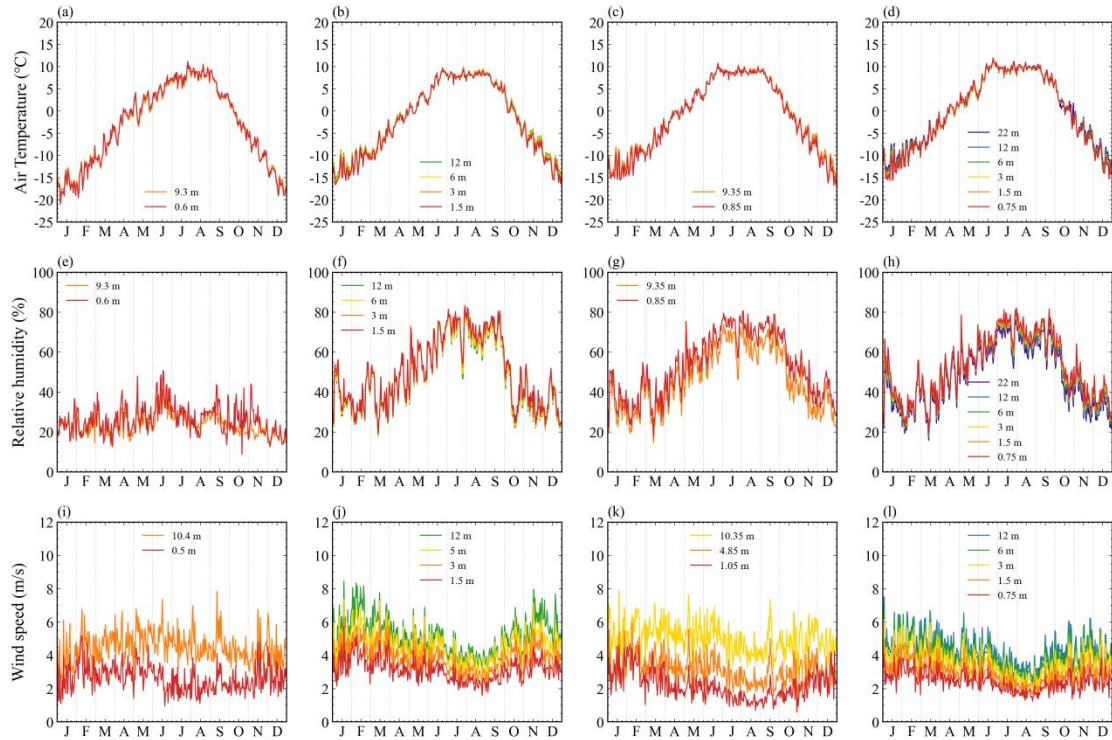
Figure 4. Daily mean of temperature at different heights of the PBL tower at NewD66 (a), Amdo (b), MS3478 (c) and BJ (d), with corresponding relative humidity (efgh) and wind speed (ijkl) at each station.

Figure 4 presents an annual cycle series, comprising daily mean values derived from gradient observations. At the NewD66 station, winter temperatures are demonstrably lower than at the other stations. In summer, the peak is reached at a later point in time and the duration is shorter. Other stations reach their highest temperatures in June and remain high until early September. With the onset of the monsoon season, continuous water vapour is transported from the ocean to the interior of the TP, resulting in a warming and humidification region. The stations begin to humidify rapidly in early May, reaching a peak in July with daily average relative humidity up to 80%. They then dry rapidly by the end of September, with the end of the monsoon season. The NewD66 station is a plateau bareland, and is only humid for a short period in June, the rest of the year the relative humidity is below 30%. Wind speeds at all stations show a pattern of being lower in summer and higher in winter. The TP is characterised by prevailing westerlies in winter, with daily mean wind speeds reaching 7 m/s. In contrast, the summer months are more humid with frequent changes in weather systems, resulting in average surface wind speeds of less than 4 m/s. Wind speeds at the NewD66 station are lower in winter than at other stations, but higher in summer.

Wind directions at the TP differ significantly between the monsoon and non-monsoon seasons (Fig. 5). Influenced by the South Asian and East Asian summer monsoons, northeast winds dominate during the monsoon season, accounting for 39% of the observations. In winter, there are fewer weather systems and most of the winds are steady westerly winds, with westerly winds accounting for up to 83% of the observations at different stations. MS3478 records different wind directions than the other stations. It has a consistently high frequency of southeast winds in both summer and winter, probably due to the surrounding topography.

273
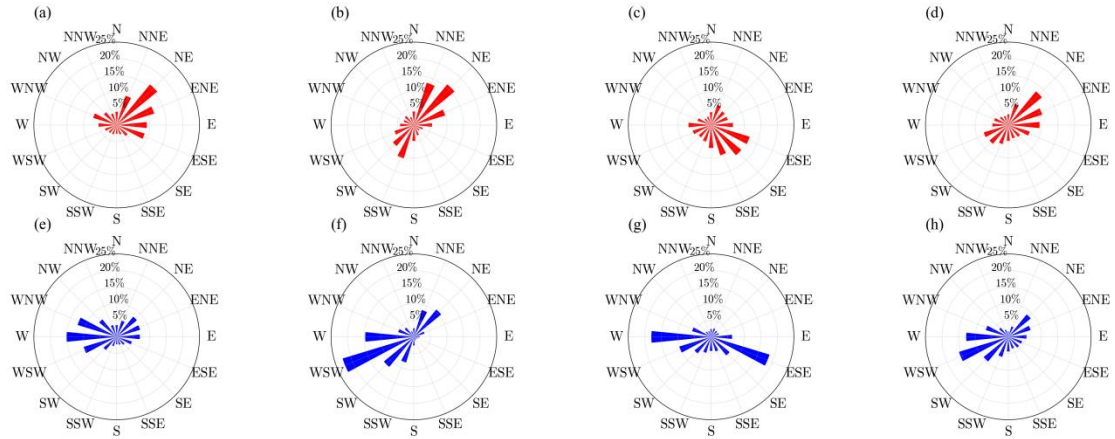
274   Figure 5. Wind direction during the monsoon season at NewD66 (a, 10.4 m), Amdo (b, 12.0 m),

275   MS3478 (c, 10.35 m), and BJ (d, 12.0 m), compared to their wind direction during the non-monsoon

276   season (e-h).

277 **3.2 Radiation fluxes**

278   Downward shortwave radiation (Rsd) is the primary source of energy at the surface, and all

279 stations show similar diurnal patterns of Rsd. Observations indicate that the TP begins to absorb solar

280 radiation at 07:00 and stops completely at 21:00 as the sun sets (Fig. 6). The maximum Rsd occurs in

281 the afternoon and reaches 732 W/m². Seasonal variations demonstrate that Rsd is lowest in winter,

282 increases continuously until spring and peaks in May. This is followed by a decrease during the

283 monsoon season, which is likely due to the effects of frequent summer rainfall on the plateau and cloud

284 cover. Since there is little variation in Rsd, differences in upward shortwave radiation (Rsu) are mainly

285 due to variations in surface albedo. The trend in Rsu at all stations is consistent with that of Rsd, with

286 the highest values observed in May, a decrease during the summer months and the minimum in winter.

287 The start and end times of Rsu at each station align with those of Rsd, as illustrated in Figure 5c.

288 MS3478 and BJ stations exhibit slightly lower Rsu values. MS3478 is plateau wetland, and the area

289 near BJ station is a pasture with extensive vegetation cover in summer, which does not strongly reflect

290 sunlight. Consequently, the lower albedo at these two stations results in relatively lower Rsu values.

291 Longwave radiation is influenced by factors such as water vapour content, aerosol content, temperature

292 stratification and cloud thickness. It shows more pronounced seasonal variations than shortwave

293 radiation. The lowest levels of downward longwave radiation (Rld) are observed in winter, while the

294 highest levels are observed in summer. The diurnal variation of Rld is the smallest of the four radiation

295 components, fluctuating within a range of 45 W/m². Upward longwave radiation (Rlu) is minimal in

296 January, increases steadily until June, and stabilises at 370 W/m² during the summer months (June to

297 August). At station MS3478, Rlu is relatively lower, remaining around 350 W/m² during the summer.

298 The minimum of Rlu occurs at 08:00, coinciding with the lowest surface temperatures. The maximum

299 values occur in the afternoon and show greater diurnal variations compared to Rld, with fluctuations up

300 to 140 W/m². Net surface radiation exhibits a clear diurnal cycle, with peaks in the afternoon and

301 slightly negative values at night. This highlights the process of surface heating the atmosphere during

302 the day and cooling it at night. Annual variations show that net surface radiation is highest in summer

303 and lowest in winter.
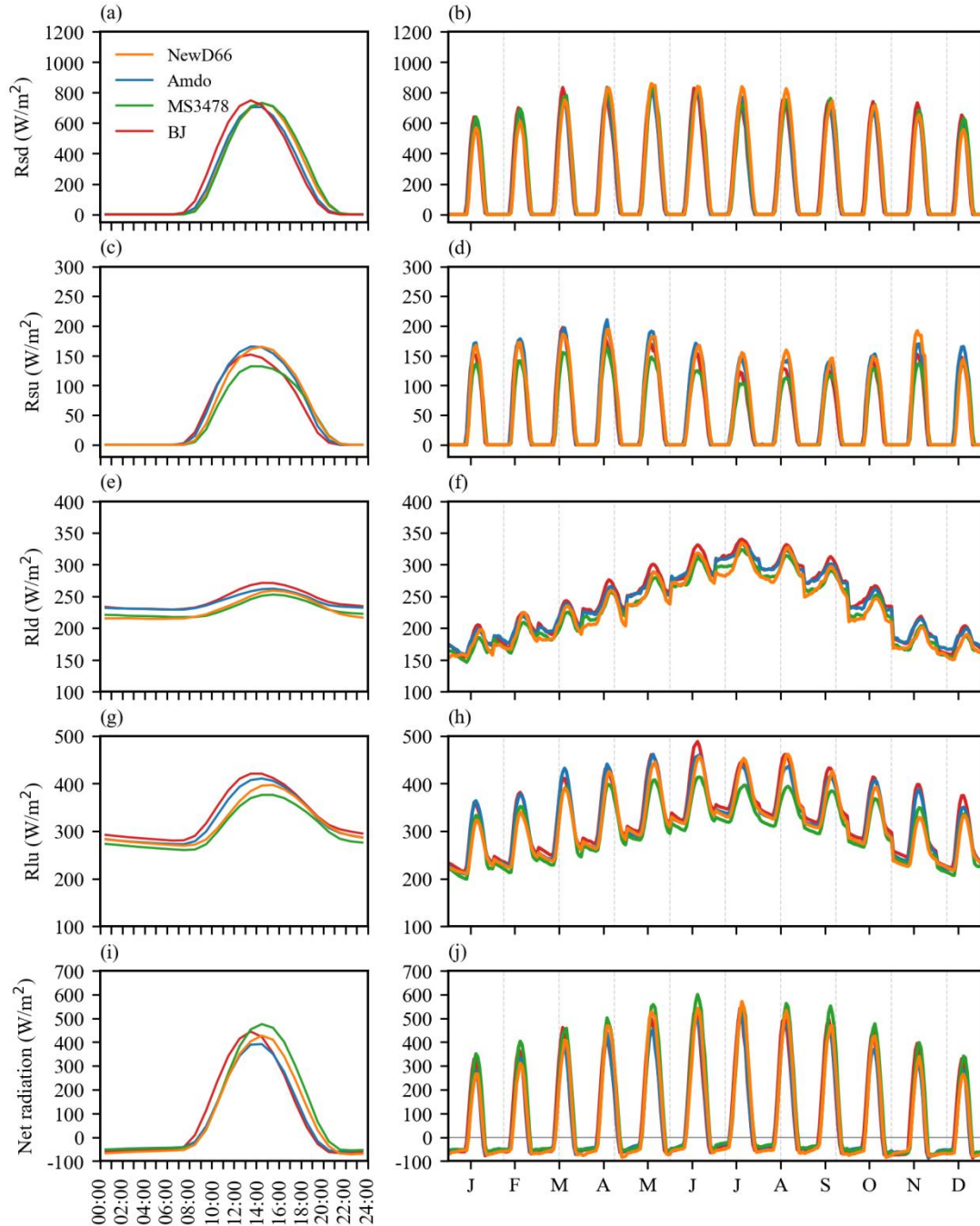
Figure 6. Diurnal variations (the first column) and monthly variations of the diurnal (the second column) downward shortwave radiation (a-b), upward shortwave radiation (c-d), downward longwave radiation (e-f), upward longwave radiation (g-h) ,and net radiation (i-j) at the 4 stations.

3.3 Surface heat flux and CO$_2$ flux

Sensible heat flux (SH) , latent heat flux (LH) and soil hear flux (SHF) are the primary forms of energy transfer between the surface and the atmosphere. Fig. 7 illustrates the monthly diurnal cycles and annual variations of SH and LH at each station. SH is influenced by the temperature difference between the surface and the atmosphere, as well as weather systems associated with precipitation, leading to numerous transient fluctuations. Seasonal variations demonstrate stronger SH at each station

in spring and weaker in summer. The daily peaks occur at 14:00, with negative values at night in winter, indicating clear temperature inversions. While net radiation increases steadily in spring, the energy absorbed by the surface before March is mainly used to melt snow. The onset of the monsoon season in May is accompanied by a rapid increase in water vapour on the TP, with a gradual dominance of LH transfer. Consequently, SH peaks in April at each station, with MS3478 (a plateau wetland) peaking in February. The Asian monsoon system transports substantial moisture into the plateau during the summer, resulting in low peaks in sensible heat flux at all stations, with a daily average of 20 W/m². In summer, the NewD66 station experiences the highest SH, while the MS3478 station experiences the lowest SH, reflecting the differences in water vapour content between the plateau bareland and plateau wetland.
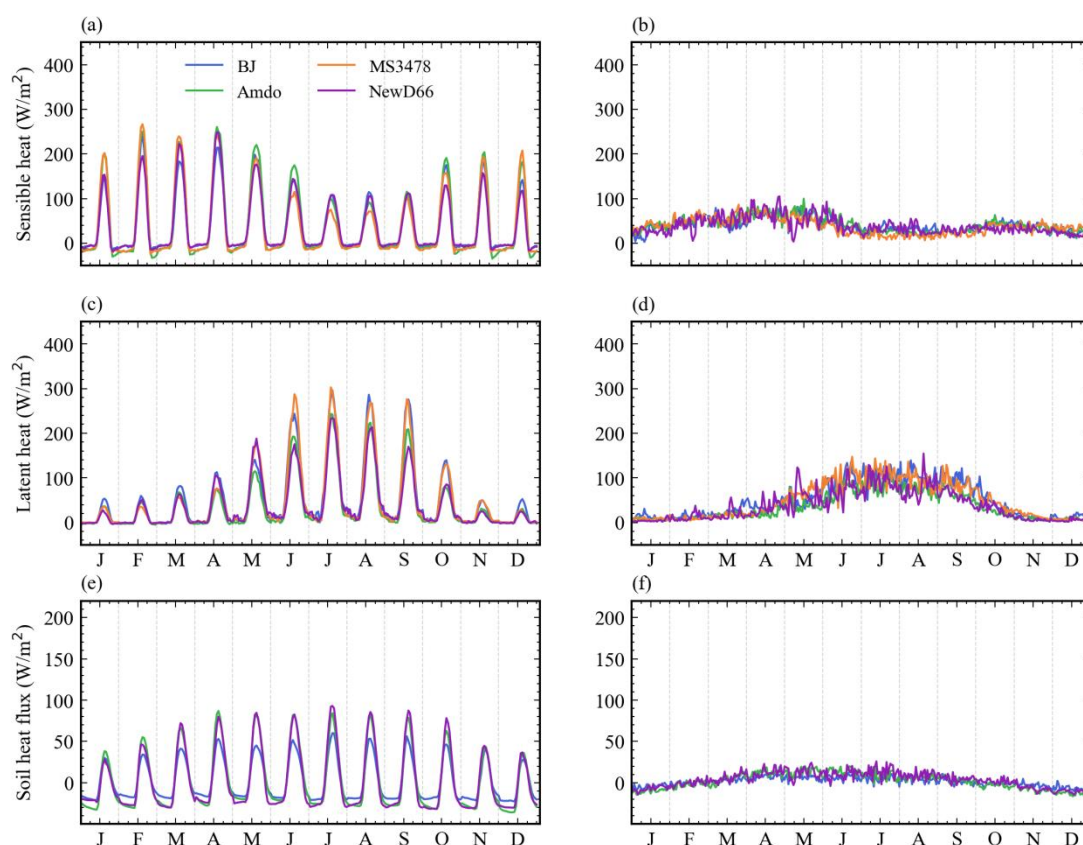
Figure 7. Monthly variations of the diurnal (the first column) and daily mean (the second column) sensible heat (a-b), latent heat (c-d), and soil heat flux (e-f) at the 4 stations.

The seasonal variation trend of LH is in opposition to that of SH. During the winter, the plateau is characterised by a relatively cold and dry climate, with LH peaks not exceeding 60 W/m² at all stations. As the monsoon season commences in May, LH rapidly rises, maintaining levels above 100 W/m² throughout the summer until it begins to decline in October. Peaks in LH occur in July at all stations, with MS3478's peak appearing earlier in June due to its higher moisture content and remaining high throughout the summer. In winter, nighttime LH approaches zero, but retains weak positive values in summer, indicating that no clear temperature inversions occur at night, and even contributing to heating the atmosphere in the early hours of the night. Fig. 7d shows significant fluctuations in LH during the summer months, which are attributed to the frequent alterations in weather patterns. The diurnal cycle of LH is also influenced by the occurrence of extreme rainfall episodes.

339 SHF is defined as the heat transfer from the land surface to deeper soil layers, is a key component
340 of the surface energy balance. As illustrated in Figure 7ef, the seasonal variation in SHF is relatively
341 moderate compared to SH and LH, with seasonal maxima remaining below 100 W/m². A clear diurnal
342 cycle is observed, characterized by a peak in the afternoon and a minimum during the night. The largest
343 diurnal variation in SHF occurred at Amdo Station from January to April. In contrast, during May to
344 September when surface thermal activity is most intense, Newd66 Station consistently exhibited high
345 levels of diurnal variability. In terms of daily mean values, SHF was highest from May to July and
346 lowest in December. It is noteworthy that Newd66 Station showed the most pronounced diurnal
347 fluctuation, which may be attributed to its plateau bareland underlying surface, which is characterised
348 by a simple composition and high sensitivity to external disturbances. Furthermore, interannual
349 variability was greatest at Newd66 Station, where the amplitude of SHF reached 40 W/m², while at BJ
350 Station, the variation was comparatively subdued, with an amplitude of only 22.7 W/m² throughout the
351 annual cycle.
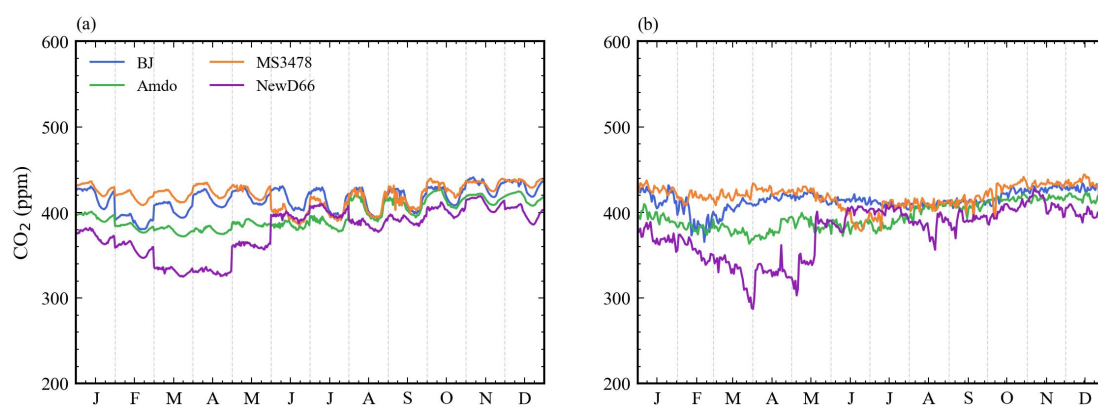
353 Figure 8. Monthly variations of the diurnal (a) and daily mean (b) CO_2 concentration at the 4 stations.

354 As shown in Figure 8a, CO_2 concentrations exhibit a diurnal cycle characterized by an increase
355 during nighttime and a decrease during daytime. This cycle shows minimal monthly variation across
356 the observation period. The NewD66 station displays only a weak diurnal signal between June and
357 August, which may be attributed to the sparse vegetation over the bareland underlying surface,
358 resulting in a relatively limited influence on local CO_2. In contrast, the diurnal cycle of CO_2
359 concentration is more pronounced at the BJ and MS3478 stations due to their dense vegetation. Figure
360 8b illustrates the annual variation in CO_2 concentration. The BJ station consistently exhibits lower CO_2
361 levels throughout the year, with more pronounced fluctuations during summer. Seasonal amplitude is
362 greater at Amdo in summer and at MS3478 in winter. The most substantial annual variation is observed
363 at NewD66, where CO_2 concentrations reach a minimum in April and peak in June.
364 **3.4 Soil hydrothermal characteristics**
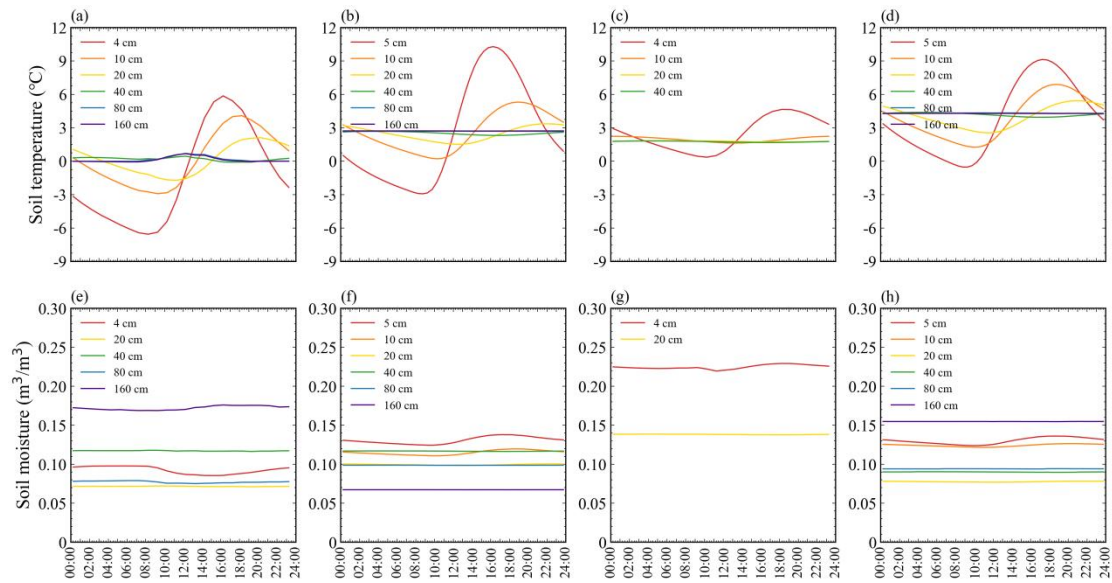
Figure 9. Layered soil temperature at NewD66 (a), Amdo (b), MS3478 (c), and BJ (d) observation, and corresponding layered soil moisture (efgh) at each station.

Soil thermal and moisture variations have a significant impact on energy and moisture exchange between the surface and the atmosphere. Due to varying observation conditions, soil observation depths differ between stations. Fig. 9 shows that all stations exhibit a diurnal cycle in soil temperature, with cooling at night and warming during the day. Soil temperature variation diminishes with increasing depth, with 4cm, 10cm, and 20cm depths showing a 2-hour delay in heating and cooling cycles. Significant spatial variation is observed due to differences in soil type, porosity, and substrate. The soil temperature at NewD66 station tends to be lower than at other sites, with 4-cm depths reaching a minimum of -6.56 ℃ at night. This is due to a lack of moisture in the surrounding air, which results in a greater daily heating effect, reaching 5.86 ℃ by 16:00. At 160 cm, a slight midday fluctuation is observed, which is not seen at other stations. MS3478, a plateau wetland, exhibits a diurnal variation of 4.29 ℃ at 4-cm depth, with a slight rise at 10 cm at 22:00, and minimal diurnal variation below 10 cm.

The diurnal cycle of soil moisture is weak at the shallowest layer, with fluctuations not exceeding 0.015 m³/m³. Below 10 cm, soil moisture shows no clear diurnal cycle. The overall soil moisture at NewD66 station is relatively low, but it does not vary linearly with depth. For example, 5-cm depth soil moisture is 0.09 m³/m³, while 160-cm depth moisture remains consistently at 0.17 m³/m³. The soil moisture data from the BJ station exhibits a comparable pattern, with slight fluctuations at the 5-cm depth, maintaining an average of approximately 0.13 m³/m³, and negligible variation at the 160-cm depth, remaining at 0.15 m³/m³. In contrast, the soil moisture at the 160-cm depth from Amdo is considerably lower than that observed in the shallow layers, likely due to the presence of a permafrost layer, which results in a consistently low liquid water content. MS3478's soil moisture exhibits no significant diurnal variation, with 4-cm depth soil moisture averaging 0.22 m³/m³ and 20-cm depth soil moisture averaging 0.13 m³/m³, which are both significantly higher than those observed at other stations.

392
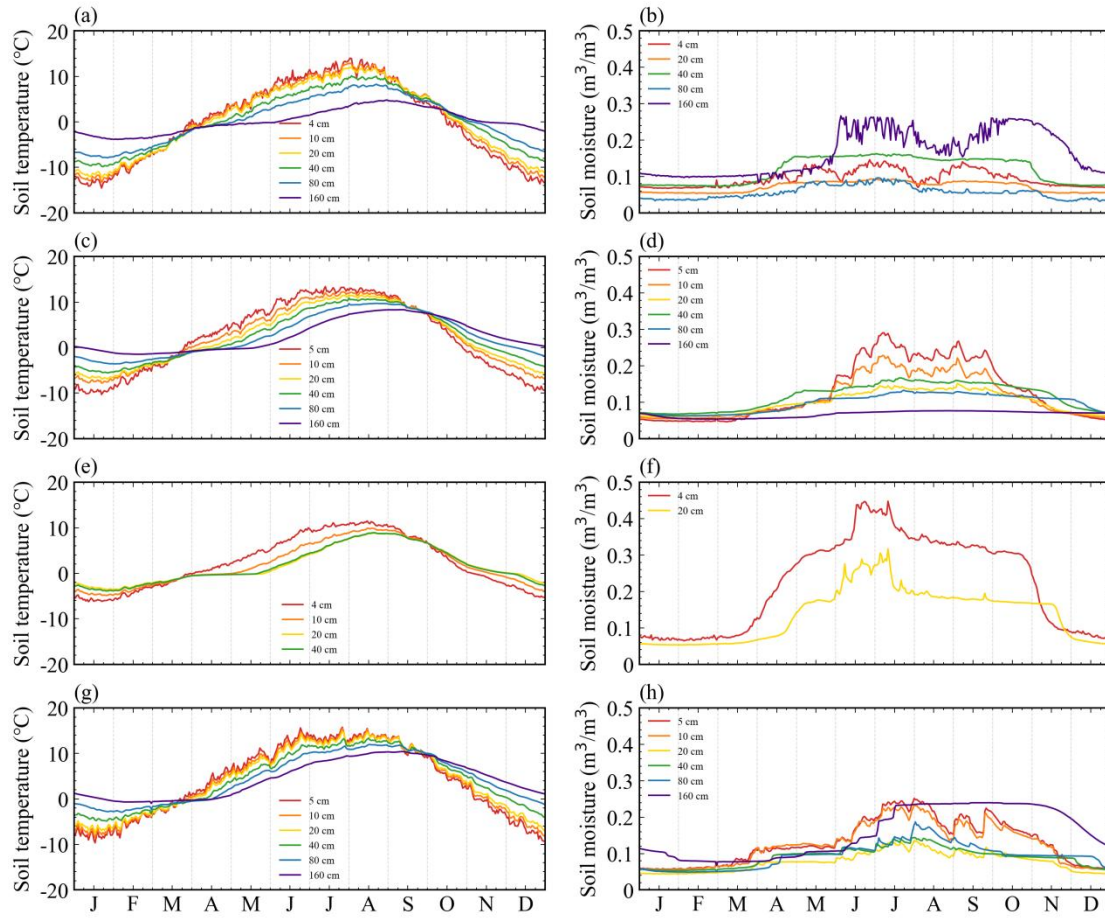
393 Figure 10. Daily mean soil temperature (a) and soil moisture (b) at NewD66,

394 same in Amdo (cd), MS3478 (ef), and BJ (gh).

395   Soil temperature and moisture exhibit clear annual variations at each station, with soil temperature

396 delaying more with increasing observation depth (Fig. 10). Surface soil temperatures peak in July, 40-

397 cm depth temperatures in August, and 160-cm depth temperatures in September. The greatest annual

398 variation in soil temperature is observed in NewD66's 4-cm depth soil temperature, reaching 28.56 ℃,

399 while the smallest is observed in MS3478's, at 17.74 ℃. A similar trend is observed in soil moisture,

400 with higher levels observed in summer and lower levels in winter. Soil moisture increases in spring due

401 to the melting of snow and ice, and in summer due to precipitation. In the absence of rainfall, surface

402 evaporation and runoff results in a rapid decrease in soil moisture. There are significant differences in

403 soil moisture between stations, with substantial fluctuations in surface moisture, indicating vertical

404 variation in the soil moisture profile. NewD66's 4-cm depth soil moisture exhibits minimal annual

405 variation, increasing by only 0.05 m³/m³ in summer. However, 160-cm depth moisture rapidly increases

406 to 0.24 m³/m³ in summer, then gradually decreases in November, coinciding with the point at which

407 160-cm depth soil temperatures exceed 0 ℃. The soil moisture at all layers of Amdo is below 0.1

408 m³/m³ in winter, with 5-cm depth moisture reaching 0.29 m³/m³ in summer, and decreasing with

409 increasing depth. MS3478's humid air contributes to higher soil moisture, with 4-cm depth moisture

410 maintaining levels above 0.3 m³/m³ from May to October, even exceeding 0.8 m³/m³ at times. BJ's 4-

411 cm depth moisture rises in April, peaking in August at 0.25 m³/m³. The lowest 20-cm depth moisture is

412 observed year-round, at only 0.12 m³/m³ in July. The 160-cm depth moisture rapidly rises in June,

413 maintaining 0.24 m³/m³ until November.

4. Data availability

Near-surface micrometeorology, soil hydrothermal characteristics, and turbulent flux observation datasets are openly available from the National Cryosphere Desert Data Center and the National Tibetan Plateau Data Center (https://www.ncdc.ac.cn/portal; https://data.tpdc.ac.cn/allData). Following a rigorous screening process that included the identification and elimination of missing values, the physical range check, and the manual quality control, valid data in CSV format is available for download. The file names adhere to the convention of station_datatype_year.csv, and all data files utilise UTC+8 as the designated time standard. Each CSV-formatted data file name includes the name of the variable, the observed height/depth, and the unit.

5. Conclusion and Discussion

As demonstrated in previous sections, the NPCE reliably reflects the characteristics of various variables across different underlying surface and temporal scales, thereby showcasing the reliability and completeness of the data. The challenging environment and dispersed stations on the CTP make it difficult to maintain equipment. Frequent extreme weather events contribute to recurrent instrument malfunctions, such as sensor drift, calibration error, environmental interference, and power supply issues. These constraints further highlight the value and importance of the data collected under such demanding conditions. The scarcity of field observation data has long been a barrier to in-depth research on the TP. Thus, long-term observations and scientific data sharing are crucial for research on the plateau. This paper introduces land-atmosphere interaction data from several observation stations centred around Nagqu. The dataset comprises 9 years (2014-2022) of hourly continuous series of near-surface meteorological, radiation, turbulent flux, and soil hydrothermal characteristics. This enables effective exploration of the entire process of land-atmosphere interactions on the plateau. Additionally, all data were manually checked for outliers and subjected to quality control. The long-term half-hourly dataset from NPCE provides the opportunity to conduct high-precision numerical simulations at the local level. This enables in-depth research to be conducted on the mechanisms by which the land and atmosphere interact on the plateau and also provides support for comprehensive research into the plateau's energy and water cycles and climate change.

The NPCE is a comprehensive research platform with the primary goal of observing and studying the impacts of weather and climate change on the Tibetan Plateau, water resource utilisation, ecological environmental protection, and human activities. The main objective of the NPCE is based on a plateau climate and the water-energy cycle. In recent years, a range of processes have been the focus of detailed analysis, including non-homogeneous terrain turbulence transfer mechanisms, radiation balance components and energy allocation processes. The analysis has been informed by long-term in situ meteorological observations (Huang et al., 2016). The spatial and temporal variability of SH and LH under complex topographic forcing is a particular highlight (Xie et al., 2018), and energy closure in the central part of the northern Tibetan plateau is further discussed (Li et al., 2015; Li et al., 2016). Satellite-derived products have been utilised to address the spatial representation limitations inherent in field observations (Ma et al., 2014; Ma et al., 2009; Ma et al., 2006). Furthermore, ground-based observations were utilised to validate and calibrate the remote sensing estimates of sensed LH, thereby improving the accuracy of the remote sensing algorithms (Zhong et al., 2019). A distributed sensor network was utilised to monitor soil temperature and humidity gradients, thereby enabling the systematic quantification of the disparities in soil moisture and heat fluxes between permafrost and

seasonal permafrost. In these areas, phase change LH associated with freeze-thaw transitions have been demonstrated to influence surface energy distribution (Liu et al., 2015; Fu et al., 2022). A comprehensive analysis of the pattern of boundary layer changes on the CTP has been conducted utilising PBL towers, as well as MWR and radiosonde data (Wang et al., 2025; Sun et al., 2021; Sun et al., 2020). The integration of multi-source observations (Near-surface meteorological data, EC system, boundary layer observation, and satellite inversion) has modified the model representation of land-atmosphere energy balance processes, and further refinement of the parameterisation scheme has been applied to soil freeze-thaw processes (Deng et al., 2021). The enhanced numerical simulation accuracy of blowing snow processes in the CLM model facilitates a more profound comprehension of surface processes and cryosphere changes in local area (Xie et al., 2023; Xie et al., 2021).

The data presented in the paper is the average result after filtering out missing values. However, in practical applications, considering the difficulty of instrument maintenance, there may inevitably be anomalies or data discontinuities. As a key observation project on the CTP, the NPCE is implementing an ambitious plan to enhance its monitoring capabilities for understanding global climate dynamics due to its high altitude and ecological sensitivity. This initiative focuses on acquiring advanced instrumentation and expanding monitoring sites to deepen insights into atmospheric, hydrological, and ecological processes, particularly in the CTP and the upper Nu River (Salween River) basin. For instrument acquisition, the station will deploy Raman lidar systems, which are highly specialized for simultaneous detection of water vapor and aerosols in the lower atmosphere. These Raman lidar systems utilize laser-based spectroscopy to provide high-resolution measurements of water vapor concentrations, enabling detailed analysis of moisture transport and its influence on regional climate patterns. Additionally, the same Raman lidar systems will measure aerosol properties, such as particle size, concentration, and distribution, which are essential for studying air quality, aerosol-cloud interactions, and their impact on radiative forcing in the plateau's unique environment. To complement these atmospheric measurements, the station will acquire advanced greenhouse gas analyzers specifically designed to monitor carbon dioxide and methane fluxes from soil and vegetation respiration, providing critical data on biogeochemical cycles and the carbon dynamics of high-altitude ecosystems under changing climatic conditions.

The site expansion plan involves establishing new monitoring stations on the CTP and the upper Nu River basin to broaden the scope of environmental observations. The CTP, with its expansive high-altitude grasslands, offers a unique setting to study the interplay between atmospheric processes and ecosystem responses to climate change. Similarly, the upper Nu River basin, a vital hydrological region, will host new sites to investigate water cycles, soil moisture dynamics, and vegetation responses to environmental shifts. By expanding coverage in the upstream Nu River, the station aims to capture spatial and temporal variations in hydrological and ecological parameters, supporting research on water resource management, ecosystem resilience, and climate adaptation strategies in this ecologically sensitive area.

Acknowledgements

This work was jointly supported by Science and Technology Projects of Xizang Autonomous Region, China (XZ202501JD0022), the National Natural Science Foundation of China (42330609, U2442207), the Youth Innovation Promotion Association of Chinese Academy of Sciences (2021427), the West Light Foundation (xbzg-zdsys-202409) of the Chinese Academy of Sciences, Key talent

502 project in Gansu and Central Guidance Fund for Local Science and Technology Development Projects
503 in Gansu (No.24ZYQA031). We also acknowledge the Computing Center in Xi'an for providing the
504 computing resources.
505

506 **Author contributions**

507 All the authors were involved in the generation of the introduced dataset. HY, GW, FS and FL wrote
508 the manuscript with contributions from all the other authors.

509

510 **References**

511

512 Bian, L., Gao Z., Ma Y., Koike T., Ma Y., Li Y., Sun J., Hu Z. and Xu X.: Seasonal Variation in
513   Turbulent Fluxes over Tibetan Plateau and Its Surrounding Areas: Research Note, Journal of
514   the Meteorological Society of Japan., 90C, 157-171, 2012.

515 Ciwangdunzhu, Du J. and Danzengcuojie: Spatial-temporal Change of Consecutive Dry Days in
516   Changtang National Nature Reserve of Tibet During 1971-2017, Chinese Agricultural Science
517   Bulletin, 34(30),118-122, 2018. (in Chinese).

518 Chen, B., Chao W. and Liu X.: Enhanced climatic warming in the Tibetan plateau due to doubling CO2:
519   A model study, Climate Dynamics, 20(4), 401–413, 2003.

520 Curio, J. and Scherer D.: Seasonality and spatial variability of dynamic precipitation controls on the
521   Tibetan Plateau, Earth System Dynamics, 7(3), 767-782, 2016.

522 Deng, M., Meng X., Lu Y., Li Z., Zhao L., Hu Z., Chen H., Shang L., Wang S. and Li Q.: Impact and
523   sensitivity analysis of soil water and heat transfer parameterizations in Community Land
524   Surface Model on the Tibetan Plateau, Journal of Advances in Modeling Earth Systems, 13(9),
525   e2021MS002670, 2021.

526 Duan, A. and Xiao Z.: Does the climate warming hiatus exist over the Tibetan Plateau? Scientific
527   reports 5(1), 13711, 2015.

528 Fan, X., Li Y. and Li L.: Synoptic-Scale Effects of Atmospheric Heat Source over Key Areas of the
529   Tibetan Plateau on Its Downstream Rainfall in Summer, Journal of Climate, 36(11), 3647-
530   3666, 2023.

531 Fu, C., Hu Z., Yang Y., Deng M., Yu H., Lu S., Wu D. and Fan W.: Responses of Soil Freeze-Thaw
532   Processes to Climate on the Tibetan Plateau from 1980 to 2016, Remote Sensing, 14(23),
533   5907, 2022.

534 Gu, L., Yao J., Hu Z. and Zhao L.: Comparison of the surface energy budget between regions of
535   seasonally frozen ground and permafrost on the Tibetan Plateau, Atmospheric Research, 153,
536   553-564, 2015.

537 Gu, L., Yao J., Hu Z., Ma Y., Sun F., Yu H., Wang S., Yang Y., Guo R. and Qin Y.: Characteristics of
538   the atmospheric boundary layer's structure and heating (cooling) rate in summer over the
539   Northern Tibetan Plateau, Atmospheric Research, 269, 106045, 2022.

540 Guo, Y., Zhang Y., Ma Y., Ma N.: Surface heat source intensity and surface water/energy balance in
541   Shuanghu, northern Tibetan Plateau, Acta Geographica Sinica, 69(07),983-992, 2014.

542 He, H., Hu Z., Xun X., Hao L., Gu L., Sun J. and Xu L.: The variation characteristics of surface
543   radiation in wetlands on the northern Tibetan Plateau, Acta Energiae Solaris Sinica,
544   31(05),561-567, 2010. (in Chinese).

545 Huang, F. and Ma W.: Analysis of Long-Term Meteorological Observation for Weather and Climate
546   Fundamental Data over the Northern Tibetan Plateau, Advances in Meteorology, 2016(1),
547   4878353, 2016.
548 Immerzeel, W., Lutz A., Andrade M., Bahl A., Biemans H., Bolch T., Hyde S., Brumby S., Davies B.,
549   Elmore A., Emmer A., Feng M., Fernández A., Haritashya U., Kargel J., Koppes M.,
550   Kraaijenbrink P., Kulkarni A., Mayewski P., Nepal S., Pacheco P., Painter T., Pellicciotti F.,
551   Rajaram H., Rupper S., Sinisalo A., Shrestha A., Viviroli D., Wada Y., Xiao C., Yao T. and
552   Baillie J.: Importance and vulnerability of the world's water towers, Nature, 577(7790), 364-
553   369, 2020.
554 Immerzeel, Van Beek L. and Bierkens M.: Climate change will affect the Asian water towers, science,
555   328(5984), 1382-1385, 2010.
556 Jin, H., He R., Cheng G., Wu Q., Wang S., Lü L. and Chang X.: Changes in frozen ground in the
557   Source Area of the Yellow River on the Qinghai–Tibet Plateau, China, and their eco-
558   environmental impacts, Environmental Research Letters, 4(4), 045206, 2009.
559 Kang, S., Xu Y., You Q., Flügel W., Pepin N. and Yao T.: Review of climate and cryospheric change
560   in the Tibetan Plateau, Environmental research letters, 5(1), 015101, 2010.
561 Lei, Y., Yang K., Wang B., Sheng Y., Bird B., Zhang G. and Tian L.: Response of inland lake
562   dynamics over the Tibetan Plateau to climate change, Climatic Change, 125, 281-290, 2014.
563 Lei, Y., Yao T., Bird B., Yang K., Zhai J. and Sheng Y.: Coherent lake growth on the central Tibetan
564   Plateau since the 1970s: Characterization and attribution, Journal of Hydrology, 483, 61-67,
565   2013.
566 Li, L., Liu Q., Zhang Y., Liu L., Ding M. and Gu C.: Spatial distribution and variation of precipitation
567   in the Qiangtang Plateau, Geographical Research, 36(11),2047-2060, 2017. (in Chinese)
568 Li, G., Chen H., Xu M., Zhao C., Zhong L., Li R., Fu Y. and Gao Y.: Impacts of topographic
569   complexity on modeling moisture transport and precipitation over the Tibetan Plateau in
570   summer, Advances in Atmospheric Sciences, 39(7), 1151-1166, 2022.
571 Li, M., Babel W., Chen X., Zhang L., Sun F., Wang B., Ma Y., Hu Z. and Foken T.: A 3-year dataset
572   of sensible and latent heat fluxes from the Tibetan Plateau, derived using eddy covariance
573   measurements, Theoretical and Applied Climatology, 122(3-4), 457-469, 2015.
574 Li, M., Su Z., Ma Y., Chen X., Zhang L. and Hu Z.: Characteristics of land-atmosphere energy and
575   turbulent fluxes over the plateau steppe in central Tibetan Plateau, Sciences in cold and arid
576   regions, 8(2), 103-115, 2016.
577 Li, W., Guo W., Qiu B., Xue Y., Hsu P. and Wei J.: Influence of Tibetan Plateau snow cover on East
578   Asian atmospheric circulation at medium-range time scales, Nature communications, 9(1),
579   4243, 2018.
580 Li, Y. and Hu Z.: A Study on Parameterization of Surface Albedo over Grassland Surface in the
581   Northern Tibetan Plateau, Advances in Atmospheric Sciences, 26(1), 161-168, 2009.
582 Liu, H., Hu Z., Yang Y., Wang Y., Sun G. and Huang R.: Simulation of the freezing-thawing processes
583   at Nagqu Area over Qinghai-Xizang Plateau, Plateau Meteorology, 34(003), 676-683, 2015.
584 Liu, X. and Chen B.: Climatic warming in the Tibetan Plateau during recent decades, International
585   Journal of Climatology: A Journal of the Royal Meteorological Society, 20(14), 1729-1742,
586   2000.

587   Liu, X., Cheng Z., Yan L. and Yin Z.: Elevation dependency of recent and future minimum surface air
588   temperature trends in the Tibetan Plateau and its surroundings, Global and Planetary Change,
589   68(3), 164–174, 2009.
590   Ma, W., Ma Y., Li M., Hu Z., Zhong L., Su Z., Ishikawa H. and Wang J.: Estimating surface fluxes
591   over the north Tibetan Plateau area with ASTER imagery, Hydrology and earth system
592   sciences, 13(1), 57-67, 2009.
593   Ma, Y., Wang Y. and Han C.: Regionalization of land surface heat fluxes over the heterogeneous
594   landscape: from the Tibetan Plateau to the Third Pole region, International Journal of Remote
595   Sensing, 39(18), 5872-5890, 2018.
596   Ma, Y., Xie Z., Chen Y., Liu S., Che T., Xu Z., Shang L., He X., Meng X., Ma W., Xu B., Zhao H.,
597   Wang J., Wu G. and Li X.: Spatially extensive long-term quality-assured land-atmosphere
598   interactions dataset over the Tibetan Plateau, Earth System Science Data Discussions, 2024, 1-
599   37, 2023.
600   Ma, Y., Yao T., Zhong L., Wang B., Xu X., Hu Z., Ma W., Sun F., Han C., Li M., Chen X., Wang J.,
601   Li Y., Gu L., Xie Z., Liu L., Sun G., Wang S., Zhou D., Zuo H., Xu C., Liu X., Wang Y. and
602   Wang Z.: Comprehensive study of energy and water exchange over the Tibetan Plateau: A
603   review and perspective: From GAME/Tibet and CAMP/Tibet to TORP, TPEORP, and
604   TPEITORP, Earth-Science Reviews, 237, 104312, 2023.
605   Ma, Y., Zhong L., Su Z., Ishikawa H., Menenti M. and Koike T.: Determination of regional
606   distributions and seasonal variations of land surface heat fluxes from Landsat-7 Enhanced
607   Thematic Mapper data over the central Tibetan Plateau area, Journal of Geophysical Research:
608   Atmospheres, 111(D10), 2006.
609   Qiu, J.: China: the third pole, Nature, 454(7203), 393-397, 2008.
610   Shen, M., Piao S., Jeong S., Zhou L., Zeng Z., Ciais P., Chen D., Huang M., Jin C., Li L., Li Y.,
611   Myneni R., Yang K., Zhang G., Zhang Y. and Yao T.: Evaporative cooling over the Tibetan
612   Plateau induced by vegetation growth, Proceedings of the National Academy of Sciences,
613   112(30), 9299-9304, 2015.
614   Shen, Y. and Xiong A.: Validation and comparison of a new gauge-based precipitation analysis over
615   mainland China, International journal of climatology, 36(1), 252-265, 2016.
616   Song, C., You S., Ke L., Liu G. and Zhong X.: Phenological variation of typical vegetation types in
617   northern Tibet and its response to climate changes, Acta Ecol. Sin, 04, 41–51, 2012.
618   Su, Y., Zhang Y., Shang L., Wang S., Hu G., Song M., Zhou K.: Root-induced alterations in soil
619   hydrothermal properties in alpine meadows of the Qinghai-Tibet Plateau, Rhizosphere, 20:
620   100451, 2021.
621   Sun, C., Xu X., Wang P., Yang D., Zhang S., Wang C. and Cai W.: The warming and wetting
622   ecological environment changes over the Qinghai-Tibetan Plateau and the driving effect of the
623   Asian summer monsoon, Journal of Tropical Meteorology, 28(1), 95-108, 2022.
624   Sun, G., Hu Z., Ma Y., Xie Z., Wang J. and Yang S.: Simulation Analysis of Local Land Atmosphere
625   Coupling in Rainy Season over a Typical Underlying Surface in the Tibetan Plateau,
626   Hydrology and Earth System Sciences, 24, 5937–5951, 2020.
627   Sun, G., Hu Z., Ma Y., Xie Z., Yang S. and Wang J.: Analysis of local land-atmosphere coupling in
628   rainy season over a typical underlying surface in Tibetan Plateau based on field measurements
629   and ERA5, Atmospheric Research, 243, 105025, 2020.

Sun, G., Hu Z., Ma Y., Xie Z., Sun F., Wang J. and Yang S.: Analysis of local land atmosphere coupling characteristics over Tibetan Plateau in the dry and rainy seasons using observational data and ERA5, Science of the Total Environment, 774, 145138, 2021.

Sun J., Qin X. and Yang J.: The response of vegetation dynamics of the different alpine grassland types to temperature and precipitation on the Tibetan Plateau, Environmental Monitoring and Assessment, 188(1): 20, 2016.

Sun, J., Yang K., Guo W., Wang Y., He J. and Lu H.: Why has the inner Tibetan Plateau become wetter since the mid-1990s? Journal of Climate, 33(19), 8507-8522, 2020.

Ueno, K., Sugimoto S., Tsutsui H., Taniguchi K., Hu Z. and Wu S.: Role Of Patchy Snow Cover On The Planetary Boundary Layer Structure During Late Winter Observed In The Central Tibetan Plateau, Journal of The Meteorological Society of Japan, 90c, 145-155, 2012.

Wang, G., Hu Z., Yu H., Sun G., Niu R. and Wang X.: Land-atmosphere coupling characteristics in summer based on microwave radiometer data at Nagqu site of Tibetan Plateau, Atmospheric Research, 320, 108074, 2025.

Wang, Y., Liu X., Lv M., Zhang Z.: Mechanisms and influencing factors of hydrothermal processes in active layer soils on the Qinghai-Tibet Plateau under freeze–thaw action, Catena, 220: 106694, 2023.Wu, G., Liu Y., Zhang Q., Duan A., Wang T., Wan R., Liu X., Li W., Wang Z. and Liang X.: The influence of mechanical and thermal forcing by the Tibetan Plateau on Asian climate, Journal of Hydrometeorology, 8(4), 770-789, 2007.

Wu, G., Liu Y., He B., Bao Q., Duan A. and Jin F.: Thermal Controls on the Asian Summer Monsoon, Scientific reports, 2(1), 404, 2012.

Xie J., Yu Y., Liu C. and Ge J.: Characteristics of Surface Sensible Heat Flux over the Qinghai-Tibetan Plateau and Its Response to Climate Change, Plateau Meteorology, 37(1), 28-42, 2018.

Xie, Z., Ma W., Ma Y., Hu Z., Sun G., Han Y., Hu W., Su R. and Fan Y.: "Decision tree-based detection of blowing snow events in the European Alps, Hydrology and earth system sciences, 25(7), 3783-3804, 2021.

Xie, Z., Ma Y., Ma W., Hu Z. and Sun G.: Comparison of varied complexity parameterizations in estimating blowing snow occurrences, Journal of Hydrology, 619, 129291, 2023.

Yang, K., He J., Tang W., Qin J. and Cheng C.: On downward shortwave and longwave radiations over high altitude regions: Observation and modeling in the Tibetan Plateau, Agricultural and Forest Meteorology, 150(1), 38-46, 2010.

Yang K., Koike T., Fujii H., Tamagawa K. and Hirose N.: Improvement of Surface Flux Parameterizations with a Turbulence-Related Length, Quarterly Journal of Royal Meteorological Society, 128(584), 2073-2087, 2002.

Yang, K., Wu H., Qin J., Lin C., Tang W. and Chen Y.: Recent climate changes over the Tibetan Plateau and their impacts on energy and water cycle: A review, Global and Planetary Change, 112, 79-91, 2014.

Yang, K., Ye B., Zhou D., Wu B., Foken T., Qin J. and Zhou Z.: Response of hydrological cycle to recent climate changes in the Tibetan Plateau, Climatic change, 109, 517-534, 2011.

Yao, T., Thompson L., Yang W., Yu W., Gao Y., Guo X., Yang X., Duan K., Zhao H., Xu B., Pu J., Lu A., Xiang Y., Kattel D. and Joswiak D.: Different glacier status with atmospheric circulations in Tibetan Plateau and surroundings, Nature climate change, 2(9), 663-667, 2012.

Zhang, G., Luo W., Chen W. and Zheng G.: A robust but variable lake expansion on the Tibetan Plateau, Science Bull, 64(18), 1306-1309, 2019.

674 Zhang, T., Wang T., Krinner G., Wang X., Gasser T., Peng S., Piao S. and Yao T.: The weakening
675    relationship between Eurasian spring snow cover and Indian summer monsoon rainfall,
676    Science advances, 5(3), eaau8932, 2019.

677 Zhao, Y., Xu X., Liu L., Zhang R., Xu H., Wang Y. and Li J.: Effects of convection over the Tibetan
678    Plateau on rainstorms downstream of the Yangtze River Basin, Atmospheric Research, 219,
679    24-35, 2019.

680 Zhong, L., Zou M., Ma Y., Huang Z., Xu K., Wang X., Ge N. and Cheng M.: Estimation of
681    downwelling shortwave and longwave radiation in the Tibetan Plateau under all-sky
682    conditions, Journal of Geophysical Research: Atmospheres, 124(21), 11086-11102, 2019.

683 Zou, M., Zhong L., Ma Y., Hu Y. and Feng L.: Estimation of actual evapotranspiration in the Nagqu
684    river basin of the Tibetan Plateau, Theoretical and Applied Climatology, 132(3-4), 1039-1047,
685    2018.

686